# Interference in Autophagosome Fusion by Rare Earth Nanoparticles Disrupts Autophagic Flux and Regulation of an Interleukin-1$\beta$ Producing Inflammasome

**Ruibin Li,[†] Zhaoxia Ji,[‡] Hongqiang Qin,[§] Xuedong Kang,[⊥] Bingbing Sun,[†] Meiying Wang,[†] Chong Hyun Chang,[‡] Xiang Wang,[‡] Haiyuan Zhang,[‡] Hanfa Zou,[§] Andre E. Nel,[*,†,‡] and Tian Xia[*,†,‡]**

[†]Division of NanoMedicine, Department of Medicine, University of California, 10833 Le Conte Avenue, Los Angeles, California 90095, United States, [‡]California NanoSystems Institute, University of California, 570 Westwood Plaza, Los Angeles, California 90095, United States, [§]CAS Key Laboratory of Separation Science for Analytical Chemistry, National Chromatographic R & A Center, Dalian Institute of Chemical Physics, Chinese Academy of Sciences (CAS), Dalian 116023, China, and [⊥]Department of Pediatrics, David Geffen School of Medicine at UCLA, Los Angeles, California 90095, United States

**ABSTRACT** Engineered nanomaterials (ENMs) including multiwall carbon nanotubes (MWCNTs) and rare earth oxide (REO) nanoparticles, which are capable of activating the NLRP3 inflammasome and inducing IL-1$\beta$ production, have the potential to cause chronic lung toxicity. Although it is known that lysosome damage is an upstream trigger in initiating this pro-inflammatory response, the same organelle is also an important homeostatic regulator of activated NLRP3 inflammasome complexes, which are engulfed by autophagosomes and then destroyed in lysosomes after fusion. Although a number of ENMs have been shown to induce autophagy, no definitive research has been done on the homeostatic regulation of the NLRP3 inflammasome during autophagic flux. We used a myeloid cell line (THP-1) and bone marrow derived macrophages (BMDM) to compare the role of autophagy in regulating inflammasome activation and IL-1$\beta$ production by MWCNTs and REO nanoparticles. THP-1 cells express a constitutively active autophagy pathway and are also known to mimic NLRP3 activation in pulmonary macrophages. We demonstrate that, while activated NLRP3 complexes could be effectively removed by autophagosome fusion in cells exposed to MWCNTs, REO nanoparticles interfered in autophagosome fusion with lysosomes. This leads to the accumulation of the REO-activated inflammasomes, resulting in robust and sustained IL-1$\beta$ production. The mechanism of REO nanoparticle interference in autophagic flux was clarified by showing that they disrupt lysosomal phosphoprotein function and interfere in the acidification that is necessary for lysosome fusion with autophagosomes. Binding of $LaPO_4$ to the REO nanoparticle surfaces leads to urchin-shaped nanoparticles collecting in the lysosomes. All considered, these data demonstrate that in contradistinction to autophagy induction by some ENMs, specific materials such as REOs interfere in autophagic flux, thereby disrupting homeostatic regulation of activated NLRP3 complexes.

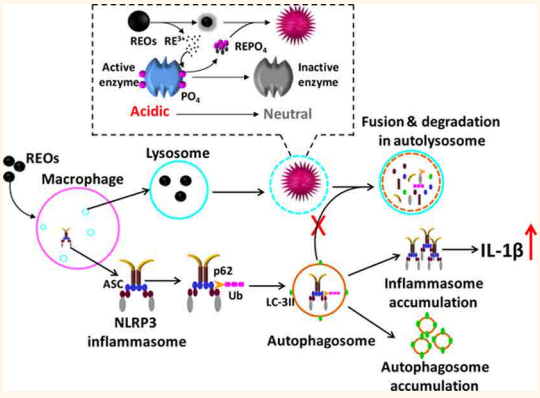


**KEYWORDS:** THP-1 · IL-1beta · carbon nanotubes · rare earth oxides · autophagy · NLRP3 inflammasome · silica

NLRP3 inflammasome activation plays an important role in particle and fiber toxicology in the lung.[1,2] In addition to the ability of occupational exposure to asbestos and quartz to induce chronic lung inflammation and fibrosis as a result of inflammasome activation, experimental studies with engineered nanomaterials (ENMs), such as carbon nanotubes (CNTs), metal oxide nanorods and rare earth oxide (REO) nanoparticles, have demonstrated that they could lead to lung injury as a result of NLRP3 inflammasome activation and IL-1$\beta$ production.[3−6] While all of the above materials are capable of inducing the assembly of the NLRP3, ASC and caspase 1 subunits secondary to lysosomal damage,[1] there are material-specific differences in precisely how the lysosomal membrane is damaged by the composition,

* Address correspondence to txia@ucla.edu, anel@mednet.ucla.edu.

Received for review June 26, 2014 and accepted September 24, 2014.

**Published online September 24, 2014**
**10.1021/nn505002w**

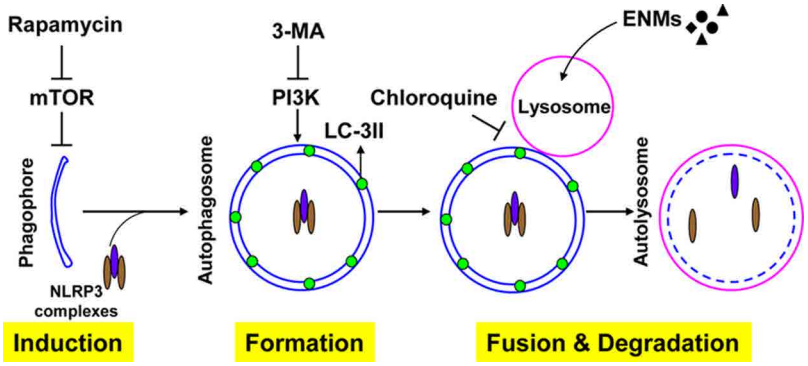


**Scheme 1. Autophagy plays a major role in clearance of activated NLRP3 inflammasome complexes. Autophagy flux involves three major steps including autophagy induction, autophagosome formation, autophagosome fusion and degradation in lysosomes. Activated NLRP3 inflammasome complexes that assemble spontaneously under basal conditions or in response to lysosomal damaging stimuli in cells are enveloped by autophagosomes and then delivered to lysosomes by a process of vesicle fusion. Subsequent degradation of inflammasomes by lysosomes serves to return IL-1$\beta$ production to basal levels. Many factors can affect these processes. mTOR inhibits autophagy induction that can be reversed by rapamycin, leading to accelerated autophagic flux. 3-Methyladenine (3-MA) inhibits autophagosome formation by inhibiting phosphatidylinositol-4,5-bisphosphate 3-kinase (PI3K) activity, while chloroquine inhibits the fusion of autophagosomes with lysosomes, leading to autophagosome accumulation. In this study, we assessed the effects of ENMs on lysosome function and autophagosome fusion. These activities may impact the NLRP3 complex degradation and IL-1$\beta$ production.**

shape/aspect ratio, redox potential and surface reactivity of the materials.[3,5,6]

Although the activation of the NLRP3 inflammasome by selected ENMs is of considerable importance in terms of material toxicity, it is also important to consider that ENMs could exert an effect on the abundance and turnover of the activated inflammasome complexes through the autophagy pathway.[7] It is known that a variety of ENMs (such as REOs, single wall CNTs, and quantum dots) are inducers of autophagy,[8−13] which in addition to its role in cellular starvation, also plays a role in mopping up and delivery of ubiquitinated protein complexes and organelles (*e.g.*, mitochondria) to the lysosome for clearance (Scheme 1).[7,14−16] It is therefore of interest to know whether the materials that are associated with NLRP3 inflammasome activation following lysosome damage can also influence the homeostatic removal of the activated complexes. This could be one of the major connections of ENMs with the autophagy pathway in that autophagy speeds up homeostatic removal of activated inflammasome complexes, with the implication that interference in autophagogic flux could lead to exaggerated IL-1$\beta$ production. Not only could this information be important from the perspective of the toxicological effects of ENMs, but it is well-known that autophagy deregulation is involved in a variety of human diseases such as cancer, Parkinson's disease, diabetes, *etc.*[16,17]

In this study, we compared REO nanoparticles with MWCNTs, both of which act as NLRP3 inflammasome inducers[3,4] and therefore establish a background against which the similarities or differences of the homeostatic regulation of IL-1$\beta$ production could be assessed. The THP-1 myeloid cell line contains a constitutively active autophagy pathway that is capable of shuttling activated NLRP3 inflammasome complexes to the lysosome during exposure to uric acid crystals, nigericin or poly(dA:dT), as demonstrated by Shi *et al.*[15] While REO nanoparticles and MWCNTs induced NLRP3 inflammasome activation and IL-1$\beta$ production, there was a dramatic difference in the magnitude of this pro-inflammatory response due to different effects of these materials on autophagic flux. While REOs interfered in autophagosome fusion with lysosomes, leading to the accumulation of activated NLRP3 complexes, MWCNTs did not interfere in autophagic flux. These results demonstrate that in addition to considering the effect of ENMs on the autophagy induction, we also need to consider the potential of interference in autophagic flux, especially the fusion of autophagosomes with lysosomes. Our research also explored the specific mechanism by which REOs disrupts autophagosome fusion by impacting key functions in the lysosome.

## RESULTS

**Characterization of Selected ENMs.** We selected a range of REO nanoparticles ($La_2O_3$, $Gd_2O_3$, $Sm_2O_3$, and $Yb_2O_3$) and as prepared (AP) MWCNTs for a comparative study of the role of autophagy in regulating the NLRP3 inflammasome. Two metal oxide (MOx) nanoparticles, $Bi_2O_3$ and $TiO_2$ were included as a control for the REO effects; while carboxylated (COOH) MWCNTs, which are poor inducers of IL-1$\beta$ production, were used as a negative control for AP-MWCNTs. Crystalline silica (quartz) was used as a positive control for NLRP3 inflammasome activation, while mesoporous silica nanoparticles (MSNP) served as negative control. All materials were fully characterized for size, zeta potential and hydrodynamic diameter. The REOs, $TiO_2$ and $Bi_2O_3$ are spherical nanoparticles with primary sizes ranging from 15 to 186 nm (Figure 1). The AP-MWCNTs

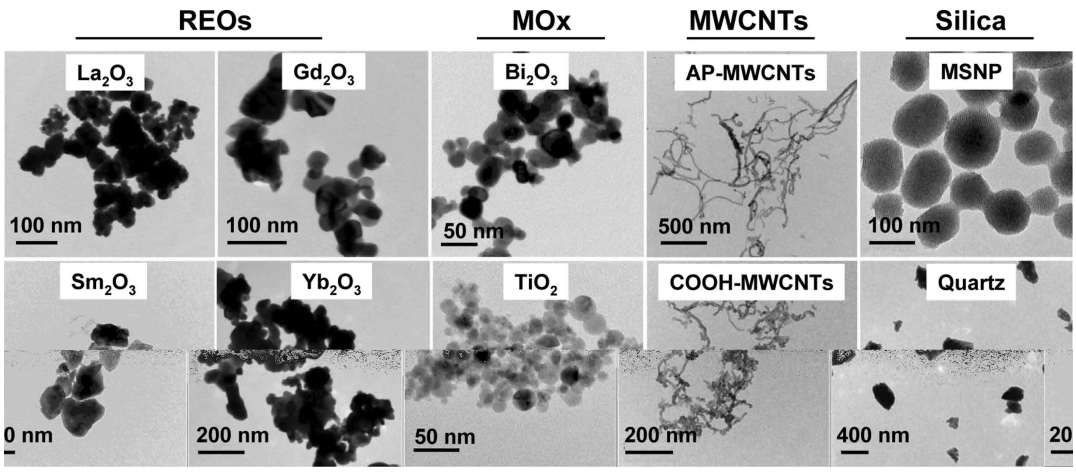


**Figure 1. TEM images of ENMs. The particles were suspended in $H_2O$ to prepare grids for TEM imaging. This imaging was performed in the UCLA BRI electron microscope core on a JEOL TEM at 80 kV.**

are slightly longer than COOH-MWCNTs because of fracture of the tubes during carboxylation. The irregular shaped quartz crystals were ~400 nm, while the MSNP were ~120 nm in primary size. All of these materials tended to agglomerate in deionized water and in the presence of RPMI 1640, leading to the formation of particles and tubes that exhibit hydrodynamic diameters ranging from 300 to 1000 nm (Table S1, Supporting Information).

**REO Nanoparticles Are More Potent Inducers of IL-1$\beta$ Production than MWCNTs in THP-1 Cells and Bone Marrow Derived Macrophages (BMDM).** NLRP3 inflammasome activation was determined by an ELISA to measure IL-1$\beta$ release in cell supernatants. As shown in Figure S1, REOs, AP-MWCNTs and quartz induced significantly higher IL-1$\beta$ production in wild-type THP-1 cells than the control particles. The role of the NLRP3 inflammasome in this pro-inflammatory response was demonstrated by the lack of IL-1$\beta$ production in NLRP3- and ASC-deficient THP-1 cells (Figure S1), similar to what we have shown previously.[3,4,18] Moreover, $La_2O_3$, $Gd_2O_3$, $Sm_2O_3$, and $Yb_2O_3$ nanoparticles induced significantly more IL-1$\beta$ production than AP-MWCNTs or quartz over an extensive material dose range (0−200 $\mu$g/mL) (Figure 2A). Similar results were obtained in primary BMDM (Figure 2B). Please notice that in the latter assay, we included $CeO_2$ in the list of REO test materials to demonstrate that, different to other REOs, IL-1$\beta$ production is not impacted by $CeO_2$ due to its reduced solubility, as previously reported by us.[3]

**REO Nanoparticles Differ from MWCNTs in Their Ability to Induce Autophagosome Accumulation in THP-1 Cells and BMDM.** Autophagy is a well-known response to cellular starvation and injury during which subcellular organelles and protein aggregates are surrounded by a double membrane to form an organelle known as the autophagosome.[19] Ubiquitinated protein complexes act as stimuli for autophagosome formation, which involves the assembly of lipidated LC3-II complexes in

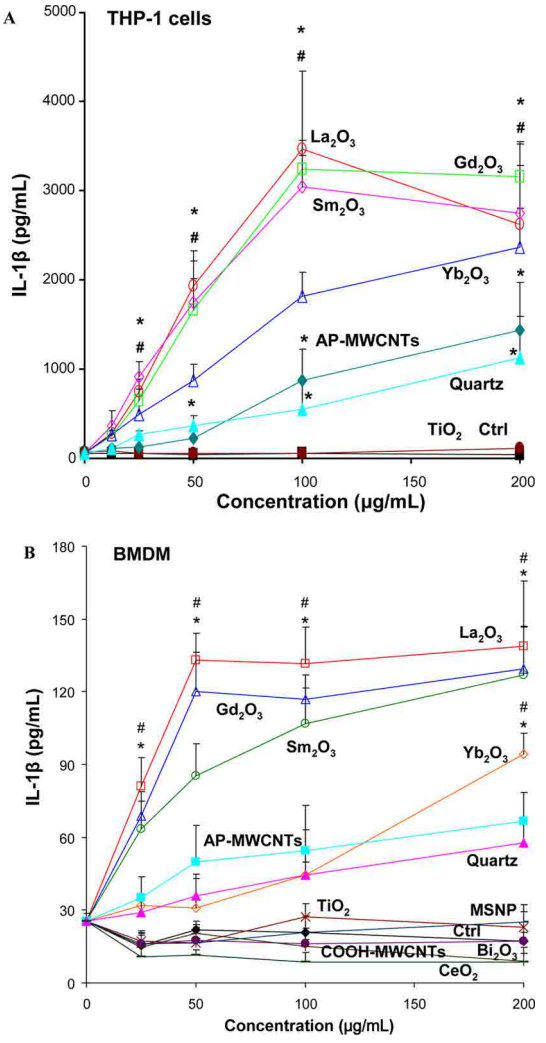


**Figure 2. IL-1$\beta$ production in THP-1 cells and BMDM in response to ENMs. IL-1$\beta$ production in (A) THP-1 cells and (B) BMDM. THP-1 cells and BMDM were exposed to 0−200 $\mu$g/mL ENMs for 24 h to determine IL-1$\beta$ release into the supernatants by ELISA. Control cells were not subjected to ENM exposure. *$p$ < 0.05 compared to AP-MWCNTs and quartz. *$p$ < 0.05 compared to control cells, $^{\#}p$ < 0.05 compared to AP-MWCNTs and quartz treated cells.**

the cytosol. This process is regulated by phosphoinositide-3-kinase (PI-3K) and autophagy-related genes (Atgs).[20] After engulfing intracellular molecules and organelles, further fusion of autophagosomes with lysosomes results in the degradation of cellular components, which serve as a new source of food or cleaning up unwanted ubiquitin-tagged proteins and organelles. From the perspective of activated NLRP3 inflammasomes, autophagy plays an important role in the removal of activated NLRP3 complexes,[15] and could therefore determine the magnitude of the IL-1$\beta$ response in MWCNTs and REO nanoparticle-exposed cells. In order to study the assembly of autophagosomes in cells exposed to these materials or pharmacological stimuli, we used a stable transfected THP-1 cell line to study the formation of GFP-LC3 labeled autophagosomes by confocal microscopy (Figure 3A).[15] The overall importance of autophagy in NLRP3 removal is demonstrated by the robust and sustained IL-1$\beta$ production in THP-1 cells treated with the PI-3 kinase as well as autophagy inhibitor, 3-methyladenine (3-MA) (Figure 3B). While all REO nanoparticles ($La_2O_3$, $Sm_2O_3$, $Gd_2O_3$ and $Yb_2O_3$) induced the appearance of GFP-labeled autophagosomes, MWCNTs (AP as well as COOH), quartz, MSNP, and metal oxides ($TiO_2$ and $Bi_2O_3$) had little or no effect on the autophagosome formation (Figure 3A). Quantitative estimation of autophagosome expression confirmed an increase in the % GFP-positive cells during REO exposure (Figure 3B); we also showed that this effect is dose- and time-dependent (Figure 3C and Figure S2). In addition, similar findings were obtained in BMDM by staining of autophagosomes with FITC-labeled anti-LC-3II. REO particles induced significant autophagosome accumulation compared to other particle types, including $CeO_2$ (Figure S3). Interestingly, there was no increase in % GFP-positive THP-1 cells in response to the introduction of an mTORC1 inhibitor, rapamycin (Rapa), which leads to autophagy induction (Figure 3B). Rapa also failed to induce IL-1$\beta$ production (Figure 3B). This suggests that the major effect of REO nanoparticles is inhibition of autophagic flux but not autophagy induction. Noteworthy, chloroquine (CQ), which acts as an inhibitor of autophagosome fusion as a result of interference in lysosome acidification,[20] resulted in a visually identical accumulation of GFP-LC3 complexes in THP-1 cells (Figure 3A and 3B).

The accumulation of LC3 complexes in response to $La_2O_3$ (as a representative REO) was confirmed by Western blotting (Figure 4). Immunoblotting to assess the abundance of lipidated LC3-II complexes in THP-1 extracts demonstrated that $La_2O_3$ (similar to CQ) increased LC3-II abundance in the cell (Figure 4A). In contrast, AP-MWCNTs and quartz had no effect on LC3-II assembly. We also used TEM to look at cellular vacuoles that exhibit the ultrastructural features of

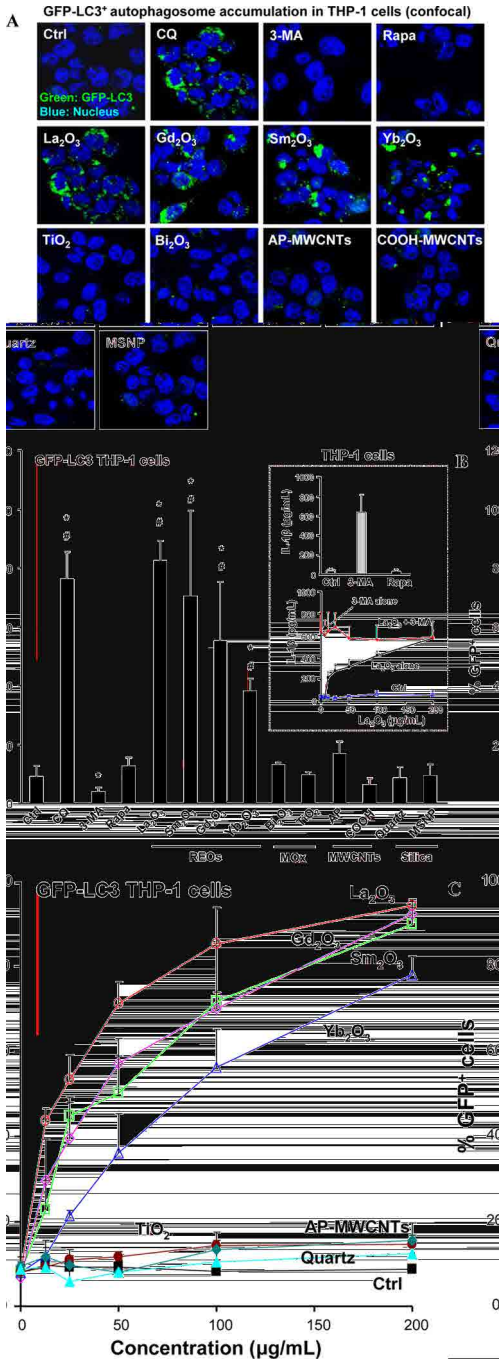


**Figure 3. Confocal microscopy to assess autophagosome accumulation in response to ENM exposure in GFP-LC3$^+$ THP-1 cells. (A) Confocal microscopy to assess GFP fluorescence in the stable transfected cells exposed to 50 $\mu$g/mL of ENMs, 5 mM 3-MA, 50 nM Rapa or 50 $\mu$g/mL CQ for 24 h. Cellular nuclei were stained with Hoechst dye. Confocal microscopy was carried out with a Leica Confocal SP2 1P/FCS. (B) The % cells expressing fluorescent autophagosomes was calculated by counting the number of cells expressing three GFP-LC3$^+$ dots or one prominent dot. The graphs that were inserted are intended to show the comparative IL-1$\beta$ production in this THP-1 cell line in response to treatment with 3-MA or Rapa for 6 h (upper panel), or $La_2O_3$ plus or minus 3-MA for the same duration. (C) Dose−response analysis to determine autophagosome accumulation in response to ENM treatment for 24 h over a 200 $\mu$g/mL dose range. *$p < 0.05$ compared to Ctrl cells, $^{\#}p < 0.05$ compared to AP-MWCNTs or quartz treated cells.**

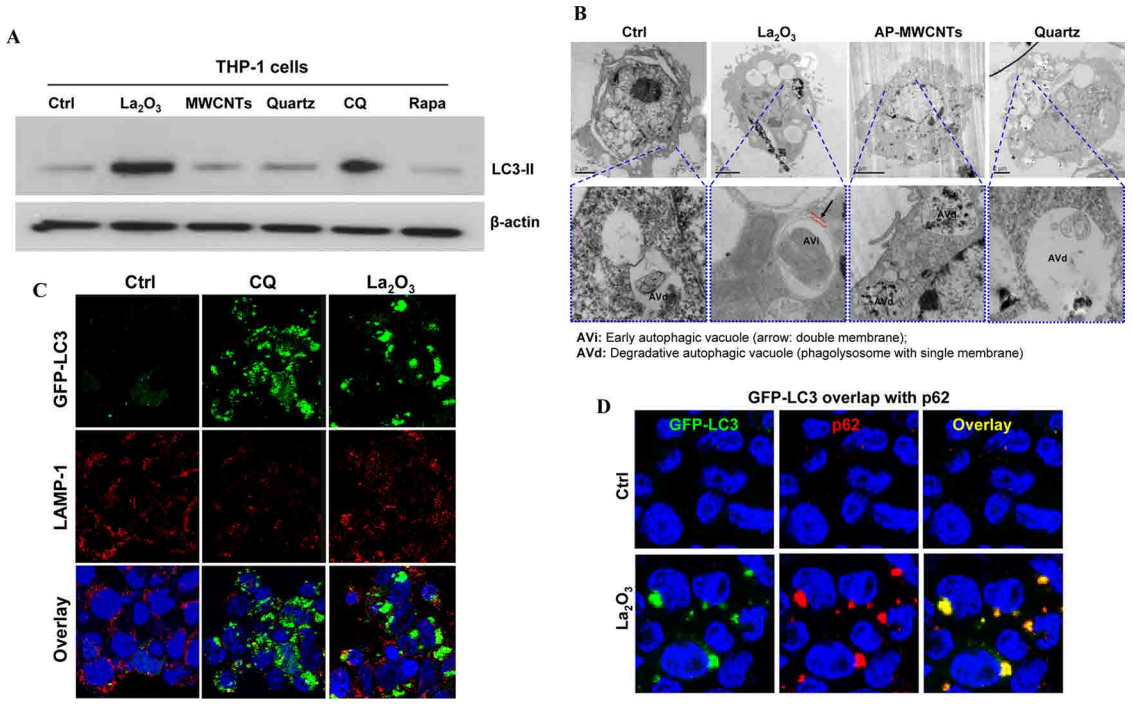


**Figure 4. Determination of autophagy blockade by $La_2O_3$ in THP-1 cells, using immunoblotting, TEM and confocal microscopy. (A) Quantification of LC3-II expression in ENM-treated THP-1 cells by Western blotting. THP-1 cells were treated with 50 $\mu$g/mL of each ENM, 50 $\mu$g/mL CQ or 50 ng/mL Rapa for 24 h. Immunoblotting was performed as described in Materials and Methods. Please notice that we do not detect the express of LC3-I in THP-1 cells by immunoblotting; however, we did observe LC3-I expression in HeLa cells (data not shown), which is not surprising because the expression of LC3-I depends on cell types.[49,50] (B) Visualization of early and degradative autophagosomes in ENM-treated THP-1 cells by TEM. THP-1 cells were exposed to 50 $\mu$g/mL REOs, AP-MWCNTs and quartz for 24 h. Cells were washed and fixed with 2% glutaraldehyde to prepare TEM sections. (C) Confocal microscopy to show colocalization of GFP-LC3 with LAMP-1 in GFP-LC3$^+$ THP-1 cells. Calculation of the % colocalization by ImageJ software demonstrated that the coefficient in $La_2O_3$ treated cells was less than 30%. (D) Confocal microscopy to demonstrate the localization of p62 in GFP-LC3$^+$ THP-1 cells, which were treated with 50 $\mu$g/mL $La_2O_3$ or 50 $\mu$g/mL CQ for 24 h. The cells were fixed, permeabilized, and stained with Hoechst, Texas Red labeled LAMP-1 or p62 antibody before confocal microscopy.**

early (immature) or late (degradative) autophagosomes; these structures can be distinguished based on the surrounding membrane and vacuolar content (Figure 4B). Thus, while immature autophagic vacuoles (AVi) are characterized by the presence of a double lipid bilayer that contains an electron-lucent cleft and is translucent, nondigested cellular components (such as ribosomes or endoplasmic reticulum), the degradative vacuoles (AVd) are lined by a single membrane that surrounds partially degraded, electron-dense cellular material.[20] TEM analysis demonstrated that while it was possible to discern the presence of AVi in $La_2O_3$ treated cells, it was not possible to observe AVd vacuoles (Figure 4B). However, AVd vacuoles could clearly be seen to be present in untreated cells or cells exposed to AP-MWCNTs or quartz (Figure 4B).

Further demonstration of the failure of autophagosomes to fuse with lysosomes in $La_2O_3$ or CQ-treated THP-1 cells was provided by confocal microscopy, which failed to demonstrate colocalization of the accumulated GFP-LC3 complexes with LAMP-1$^+$ lysosomes (Figure 4C). One mechanism by which intracellular protein complexes and organelles are tagged for delivery to autophagosomes is through binding to the adaptor protein, p62, which recognizes polyubiquitinated targets and also bind to LC3 through its LC3-interaction region (LIR).[21] It is known that NLRP3-bound ASC complexes undergo ubiquitination.[15] After the delivery of ubiquitinated targets to lysosomes, p62 is degraded.[21] Use of fluorescence staining and confocal microscopy demonstrated that the sites of p62 accumulation correspond to the intracellular location of GFP-LC3 complexes in $La_2O_3$-treated THP-1 cells (Figure 4D). ImageJ software confirmed that the % colocalization of GFP-LC3 complexes with p62 was >95%.

All considered, the above data indicate that the REOs induce autophagosome accumulation in THP-1 cells. This leads to exaggerated IL-1$\beta$ production as a result of failure to remove assembled NLRP3 complexes. However, while AP-MWCNTs were capable of inducing inflammasome activation, this cellular response was not accompanied by autophagosome accumulation. This suggests that the major effect of the REOs is on autophagy inhibition rather than autophagy induction, as can be seen for some ENMs.[7] This notion was confirmed by looking at mTORC1 phosphorylation at serine 2448 in THP-1 cells treated with Rapa or exposed to $La_2O_3$, AP-MWCNT, and

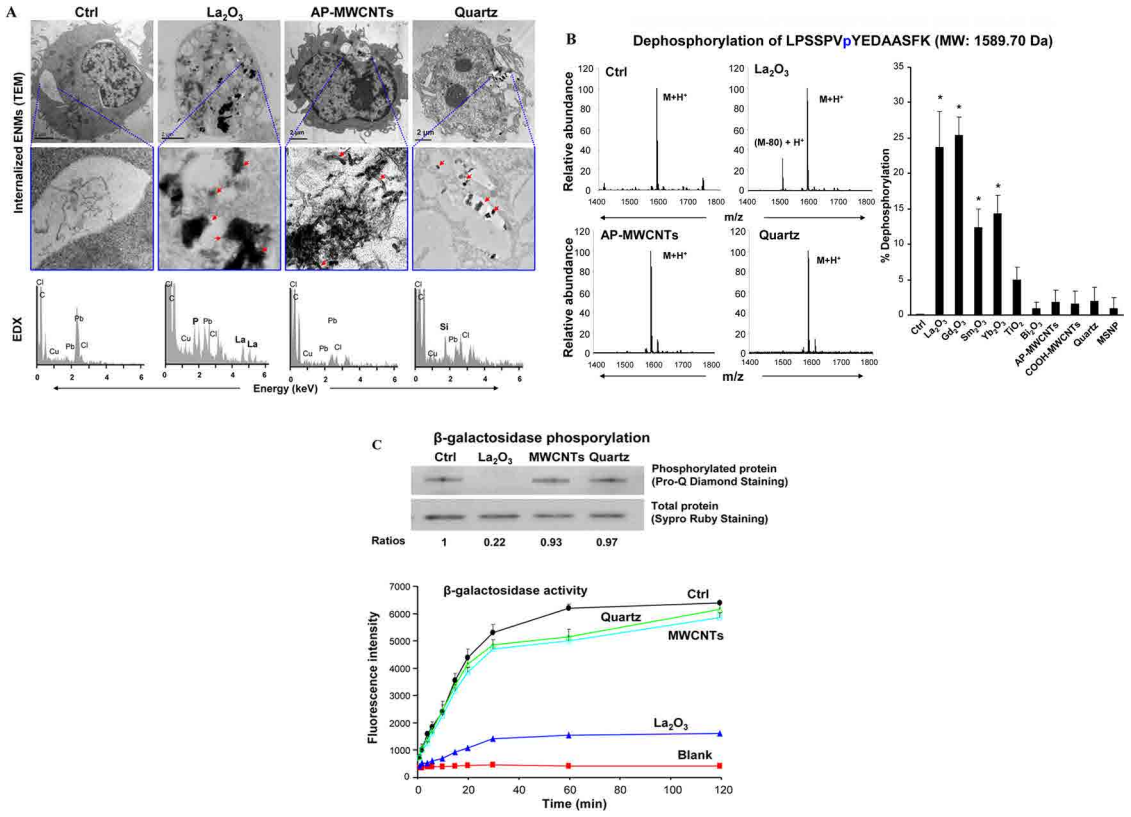


**Figure 5. Subcellular localization of ENMs by TEM and the effect on protein phosphorylation in exposed THP-1 cells. (A) Subcellular distribution of $La_2O_3$, AP-MWCNTs and quartz by TEM. THP-1 cells were exposed to 50 $\mu$g/mL nanoparticles for 24 h and then subjected to TEM as described in Figure 4. EDX was used to determine the elemental composition of the ENMs in the cells. (B) Dephosphorylation of LPSSPVpYEDAASFK by ENMs. The phosphorylation of this peptide was determined by MALDI-TOF/TOF spectrometry, in which we used the ratios of the peak intensities before and after ENMs treatment to determine the % dephosphorylation. (C) Determining the effect of dephosphorylation on the enzymatic activity of $\beta$-galactosidase before and after exposure to $La_2O_3$, AP-MWCNTs or quartz. Phosphorylation was determined by Pro-Q-Diamond and Sypro Ruby staining, while enzymatic activity was determined through the use of a fluorescent substrate. *$p < 0.05$ compared to non-REO particles.**

quartz. mTORC1 phosphorylation inhibits autophagy, while interference in the phosphorylation of this residue by Rapa stimulates autophagy induction.[22] As shown in the phosphoprotein immunoblot in Figure S4, Rapa prevented S2448 phosphorylation while $La_2O_3$, MWCNTs and quartz failed to impact mTORC1 phosphorylation. This confirms that autophagy induction does not contribute significantly to autophagic flux in $La_2O_3$-treated THP-1 cells.

**The Inhibition of Autophagosome Fusion by REOs Involves Effects on Lysosome Acidification and Disruption of Structural Phosphates in the Lysosome.** To determine how $La_2O_3$ may interfere in autophagosome fusion, we followed the intracellular fate of our study materials by TEM. As shown in Figure 5A, these materials were taken up into lysosomes as previously shown by our groups and others.[3,23,24] Interestingly, the spherical $La_2O_3$ nanoparticles transformed into urchin-shaped structures in lysosomes (Figure 5A), with EDX analysis demonstrating that this transformation is accompanied by the acquisition of $LaPO_4$ on the particles (Figure 5A). In addition, other REOs ($Gd_2O_3$, $Sm_2O_3$ and $Yb_2O_3$) also transformed in lysosomes and showed urchin-shaped or mesh-like structures constituted by $REPO_4$ (Figure S5A). This is consistent with our previous demonstration that slow dissolution of RE ions from the particles (under acidic conditions), leading to $REPO_4$ deposition on the particle surface.[3] This transformation could be replicated under abiotic conditions where particles were incubated in an acidic phagolysosomal simulation fluid (PSF) (Figure S5B); XRD analysis confirmed the presence of $LaPO_4$. No morphological transformation was seen with either MWCNTs or quartz in cells (Figure 5A) or PSF (Figure S5B).

We asked whether phosphate complexation to $La_2O_3$ particle surfaces may deprive the lysosome of structural or functional important phosphoproteins. A commercial kit for lysosome purification was used to prepare THP-1 lysosomal extracts. Immunoblotting for the presence of LAMP-1 and cathepsin D demonstrated the enrichment of lysosomal components in these extracts (Figure S6). Electrophoretic separation of the lysosomal extracts on 2-D gels, followed by Pro-Q-Diamond staining to identify phosphoproteins, demonstrated that treatment with $La_2O_3$ nanoparticles could induce widespread dephosphorylation

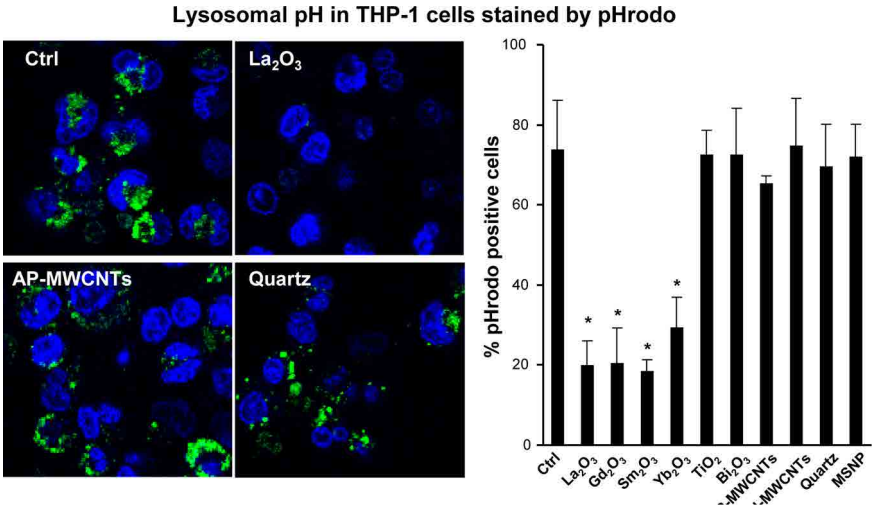


**Figure 6. Lysosomal alkalization induced by REO nanoparticles. Lysosomal pH levels induced by ENMs were determined by confocal microscopy. THP-1 cells were incubated with 50 $\mu$g/mL particles for 24 h, and then stained with a pH sensitive dye, pHrodo green dextran (50 $\mu$g/mL) in complete RPMI 1640 medium (pH, 7.4) for visualization under a confocal microscope. *$p < 0.05$ compared to untreated cells.**

of lysosomal proteins compared to extracts prepared from nontreated cells (Figure S6). Proteome analysis of spots cut from these gels demonstrated the removal of phosphates from constitutive phosphoproteins. To demonstrate the dephosphorylation more specifically, we used a custom phosphopeptide (LPSSPVpYEDAASFK, MW: 1589.70 Da), and abiotic exposure to REO nanoparticles resulted in an 80 MW decrease of the peptide as determined by matrix-assisted laser desorption/ionization time-of-flight tandem (MALDI-TOF) (Figure 5B and Figure S7). Overall we could demonstrate the loss of the phosphate group from 12−25% of the phosphopeptides treated with REOs ($La_2O_3$, $Gd_2O_3$, $Sm_2O_3$, $Yb_2O_3$). AP-MWCNTs and quartz did not exert similar effects. To see if $La_2O_3$ affects the function of a phosphorylation-dependent lysosomal enzyme, $\beta$-galactosidase was used for abiotic exposure to $La_2O_3$, MWCNTs and quartz for 4 h at 37 °C. Following separation by SDS-PAGE and sequential gel staining with Pro-Q-diamond (to detect the phosphoprotein) and Sypro Ruby (to detect the protein backbone), we could show that phosphate removal by $La_2O_3$ treatment could decrease $\beta$-galactosidase activity as determined by a fluorescent substrate, 4-methylumbelliferyl-$\beta$-d-galactopyranoside (Figure 5C). MWCNTs and quartz had no effect on the phosphorylation status as well as the activity of the enzyme (Figure 5C).

We know that interference in lysosomal acidification by CQ can disrupt autophagosome fusion and by so doing result in autophagosome accumulation.[25,26] This leads to the retention of NLRP3 complexes and robust IL-1$\beta$ production in CQ treated cells, as demonstrated in Figure 3B. In order to determine whether the ENMs under study could impact lysosomal pH, cellular staining with the fluorescent dye, pHrodo Green Dextran, was used to assess lysosomal pH.[27] Once taken up into the acidifying lysosomal environment, the increase in the fluorescence intensity of pHrodo results in the appearance of fluorescent green dots in untreated THP-1 cells during confocal microscopy (Figure 6). In cells treated with MWCNTs, MSNP, $TiO_2$ and $Bi_2O_3$ and quartz, there was no change in fluorescence intensity compared to control cells (Figure 6 and Figure S8). However, the fluorescence intensity of the dye did not increase in REO treated cells, suggesting that these nanoparticles interfere in lysosome acidification. The same effect could be shown by measuring the fluorescence intensity in a flow cytometer, which showed a shift to the left in REO treated cells (Figure S9).

**Inhibition of Autophagic Flux by REOs Leads to Reduced NLRP3 Inflammasome Degradation and Exaggerated IL-1$\beta$ Production.** Since autophagy plays a major role in the homeostatic regulation of activated NLRP3 complexes through lysosome degradation,[15] we were interested to see if we could demonstrate NLRP3 inflammasome accumulation in THP-1 cells treated with ENMs. This was accomplished by using immunoprecipitation (IP) and immunoblotting to determine ASC coprecipitation with NLRP3; increased ASC abundance reflects NLRP3 assembly in the activated inflammasome. First, a NLRP3 antibody, bound to Protein A/G immobilized beads, was used to capture cellular NLRP3 protein from cell lysates. After washing the immune precipitates, proteins were separated by SDS-PAGE and transferred to blotting membranes, which were overlaid with anti-ASC antibodies (Figure 7A). The blotting results demonstrated that while it was possible to recover equal amounts of NLRP3 and ASC from the lysates of untreated, quartz or MWCNT-treated cells, the ASC abundance was increased 2.6-fold in $La_2O_3$-treated cells. In 3-MA treated cells, ASC abundance increased 2.9-fold. The inability of MWCNTs and quartz to increase ASC

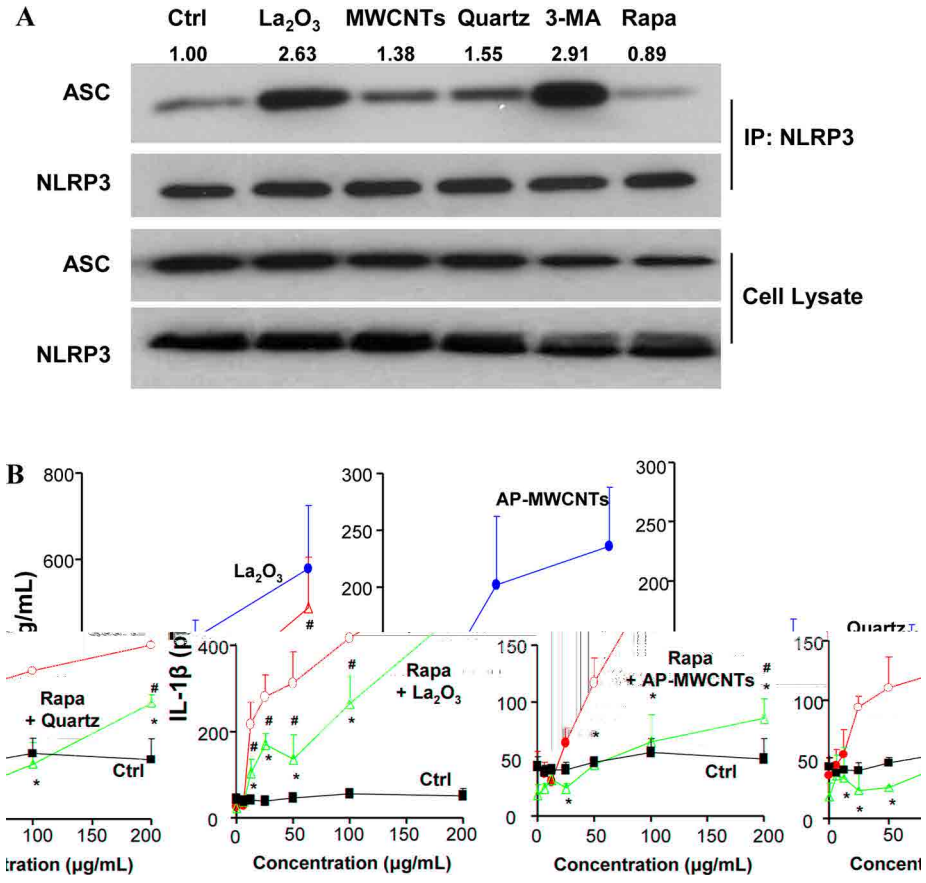


**Figure 7. REOs interfere in the degradation of NLRP3 inflammasomes by autophagy. (A) Immunoblotting to determine the relative abundance of ASC in NLRP3 immunoprecipitates obtained from THP-1 cells. THP-1 cells were treated with 50 $\mu$g/mL ENMs, 5 mM 3-MA or 50 nm Rapa for 24 h. Cells were collected and lysed before collection of the immune precipitates on beads attached to anti-NLRP3 antibodies. Subsequently, the presence of coprecipitating ASC was determined by Western blotting, as described in Materials and Methods. (B) Assessment of IL-1$\beta$ production in THP-1 cells treated with 0 to 200 $\mu$g/mL $La_2O_3$, AP tubes or quartz 3 h after prior treatment with 50 ng/mL Rapa (to speed up the autophagic flux). *$p < 0.05$ compared to untreated cells, $^{\#}p < 0.05$ compared to particle treated cells.**

complexes reflects the rapid clearance of NLRP3 inflammasomes by the constitutively active autophagic pathway in THP-1 cells. This notion was substantiated by using prior Rapa treatment in THP-1 cells, which were subsequently exposed to incremental amounts of $La_2O_3$, MWCNTs and quartz before the measuring IL-1$\beta$ production (Figure 7B). Enhancement of autophagic flux by Rapa could effectively reduce IL-1$\beta$ production in MWCNT and quartz-exposed cells, but had a lesser effect in $La_2O_3$-treated cells, likely as a result of the severity of lysosome damage induced by $La_2O_3$. Similar results were obtained in BMDM, where Rapa had little effect on $La_2O_3$ and $Gd_2O_3$ induced IL-1$\beta$ production, in contrast to AP-MWCNTs and Quartz (Figure S10).

If considered together with the results in Figure 3B, we propose that the NLRP3 steady state levels in THP-1 cells are dynamically controlled by a combination of autophagy induction, autophagosome formation, and autophagosome removal, as shown in the schematic in Figure 8. Thus, by speeding up autophagy initiation by Rapa treatment, subsequent autophagic flux leads to rapid autophagosome and inflammasome removal so that there is no accumulation of activated NLRP3 complexes. In contrast, $La_2O_3$ acts as both an inducer of inflammasome assembly as well as an inhibitor of autophagosome fusion as a result of severe and unique injury to the lysosome resulting from phosphate complexation. $La_2O_3$ induces robust accumulation of activated NLRP3 complexes and IL-1$\beta$ production, which is minimally affected by autophagy initiation by Rapa. According to the scheme in Figure 8, the PI-3 kinase inhibitor, 3-MA, leads to accumulation of NLRP3 complexes because of disrupting constitutive autophagosome assembly (Figure 3B). This explains the high rate of IL-1$\beta$ production. Although AP-MWCNTs and quartz are capable of inducing the assembly of new NLRP3 complexes, there is no interference in autophagic flux, which allows Rapa to increase the rate of inflammasome removal. This explains the high rate of decline in IL-1$\beta$ production in Figure 7B.

## DISCUSSION

In this study, we demonstrate that there are key differences in the effect of two important classes of ENMs, MWCNTs and REOs, on the autophagy pathway and the implications of those differences in terms of

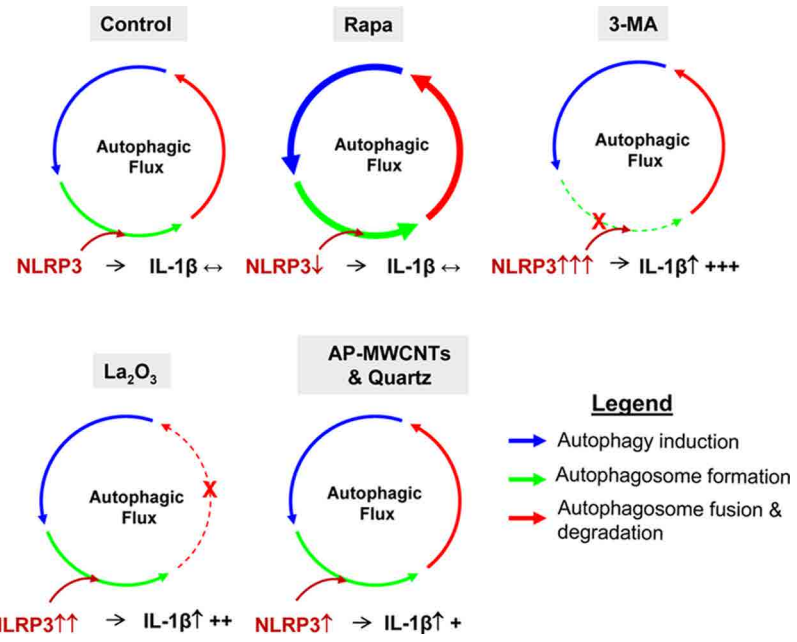


**Figure 8. Schematic to explain the effects of nanoparticles and pharmacological agents on autophagic flux and homeostatic regulation of NLRP3 complexes. Autophagic flux consists of three major steps, namely autophagy induction, autophagosome formation, and autophagosome−lysosome fusion and degradation in lysosomes. Interference on autophagic flux by ENMs or pharmacological agents could lead to deregulation of activated NLRP3 inflammasomes. Pharmacological agents, rapamycin or 3-MA, promote autophagy induction or inhibit autophagosome formation, respectively, resulting in accelerated or inhibited NLRP3 inflammasome degradation with decreased or exaggerated IL-1$\beta$ production. $La_2O_3$ blocks autophagic flux by inhibition of autophagosome−lysosome fusion, which leads to NLRP3 inflammasome accumulation and enhanced IL-1$\beta$ production. AP-MWCNTs and quartz have no effect on autophagic flux, the activated inflammasomes are degraded by autophagy with lower level of IL-1$\beta$ production than 3-MA and $La_2O_3$.**

the pro-inflammatory effects of these materials. Although exhibiting quite different sizes, shapes and surface functionalities, MWCNTs and REO nanoparticles are potent inducers of NLRP3 inflammasome assembly, which is homeostatically regulated by autophagic flux. However, while MWCNTs induced NLRP3 assembly and IL-1$\beta$ production as a result of tube-specific injury mechanisms to the lysosome, homeostatic regulation by autophagy remains intact and is capable of swiftly removing activated NLRP3 complexes. Thus, not only did MWCNTs fail to induce the accumulation of LC3-labeled autophagosomes, but fusion with the lysosome could be enhanced by the autophagy inducer, Rapa. In contrast, the REO-specific mechanism of lysosomal injury, damages this organelle to the extent that it disrupts autophagosome fusion and removal of the activated NLRP3 complexes; this leads to exaggerated IL-$\beta$ production (Figure 9). Under these conditions, Rapa had a comparatively minor effect because it could not speed up removal by the damaged lysosomes. Quartz also induced IL-1$\beta$ production that was subject to Rapa down regulation, while transition metal oxides, COOH-MWCNTs and mesoporous silica failed to affect inflammasome activation. We demonstrate a unique mechanism of lysosome damage by $La_2O_3$, which results in interference in lysosome acidification and disruption of phosphoproteins. In summary, these data show that the autophagy pathway is important as a homeostatic mechanism for removal of NLRP3 complexes induced by ENMs, with the potential to impact the severity of inflammation in addition to being of possible use for therapeutic intervention in IL-1$\beta$ mediated injury.

A variety of ENMs have been shown to be capable of inducing autophagy and nanoparticles are commonly sequestered in the autophagosomal and lysosomal compartments. These include materials such as metals (*e.g.*, Mn, Pd, Au),[28−30] metal oxides (*e.g.*, $Fe_3O_4$,[31] $Al_2O_3$,[32] and $TiO_2$[33]), REOs ($Sm_2O_3$, $Eu_2O_3$, $La_2O_3$, $Nd_2O_3$, $Y_2O_3$, $Yb_2O_3$ and $Gd_2O_3$),[8−11] carbon-based materials (*e.g.*, C60[33−36] and SWCNTs[12]), polymeric nanoparticles (*e.g.*, PAMAM dendrimers),[37] quantum dots[13] and Stober silica.[38] A variety of different mechanisms are involved, including oxidative stress (*e.g.*, fullerenes),[36] direct or indirect ubiquitination of nanomaterials (*e.g.*, $Al_2O_3$ and Au),[32,39] and inhibition of mTOR signaling (*e.g.*, dendrimers and CNTs).[12,40] While the specific role of autophagy induction by ENMs is unknown, it has been postulated that autophagy induction may represent a cellular attempt to degrade foreign materials, similar to the use of autophagy to eradicate bacteria. Alternatively, autophagy could play a role in defense against cell damage; this will be discussed later. In addition to the autophagy initiation, the current communication shows that we also have to consider the inhibition of autophagic flux by ENMs. This could induce additional cellular effects due to disruption of the autophagosome in removing damaged organelles and

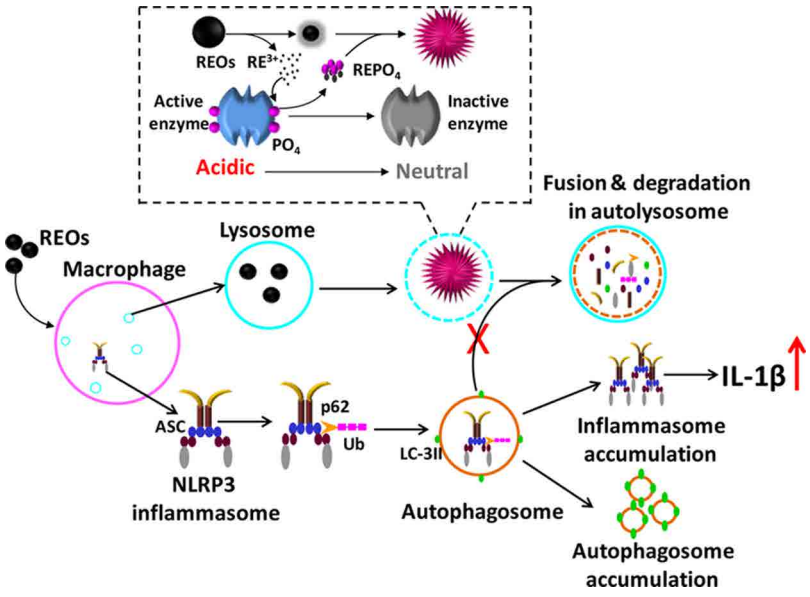


**Figure 9. Schematic to explain the effects of REOs on autophagy and NLRP3 inflammasome regulation. After internalization into lysosomes, REOs transform to RE-phosphate with sea urchin structure. This biotransformation leads to lysosomal dysfunction as manifested by the loss of enzymatic activity of lysosomal proteins as a result of dephosphorylation process and the lysosomal alkalization. Lysosomal dysfunction results in the inhibition of autophagosome–lysosome fusion, accumulation of autophagosomes and the failure to degrade the activated NLRP3 inflammasome complexes. Loss of NLRP3 inflammasome homeostasis leads to exaggerated IL-1$\beta$ production that could induce adverse health effects including lung fibrosis.**

proteins. Although limited studies with materials of gold nanoparticles[41] and SWCNTs[42] have shown interference in autophagic flux, no detailed investigation has been undertaken to show how disruption of the cleanup function of autophagy could contribute to the generation of adverse biological consequences. Our study demonstrates the importance of autophagic flux in the homeostatic regulation of activated NLRP3 inflammasomes, which if disrupted by REOs, could lead to an exaggerated inflammatory response. In contrast, MWCNTs did not exert the same effect in spite of their ability to damage lysosomes in the process of NLRP3 activation. This is likely due to the unique properties of tubes and REO nanoparticles in catalysis of lysosome injury, which serves to demonstrate that although they exhibit very different physicochemical features, there are areas of overlap from the perspective of inflammasome activation but also unique differences in the quality of the lysosomal injury so that the linked homeostatic pathway is affected very differently.

In order to explain the differences between REOs and MWCNTs, we explored the role of REO surface reactivity in lysosomal damage. After uptake into the lysosomes, REOs dissolve in the acidic environment.[3] Released RE ions exhibit high binding affinity for phosphate, with the ability to sequester phosphates from lysosomal fluid and even structural components such as phospholipids.[3] In this communication, we demonstrate that lysosomal phosphoproteins are also at risk of losing phosphates that are required for maintenance of enzyme activity. Moreover, the consumption of lysosomal protons during REO dissolution and the impact on the lysosomal proton pump (v-ATPase) may affect the alkalization of the organelle. Lysosomal acidification is critical for the fusion of autophagosomes with lysosomes, and it has previously been demonstrated that gold nanoparticles can lead to lysosomal alkalization.[41]

In addition to its role in the homeostatic regulation of NLRP3 inflammasomes, autophagy has been shown to regulate cell death. Autophagy is generally considered a pro-survival mechanism that aids the cell in dealing with stress through clearance of damaged proteins, organelles, and pathogens.[43] In agreement with this notion, recent studies have demonstrated that autophagy could directly impact apoptosis by selective degradation of pro-apoptotic proteins such as the p53 upregulated modulator of apoptosis (PUMA)[44] and the Fas-associated phosphatase 1 (FAP-1).[45] In these studies, the induction of autophagy could lead to inhibition or delay in cell death. However, there are also a growing number of studies suggesting that autophagy can promote cell death as a result of excessive degradation of cellular components such as antioxidant enzymes or mitochondria.[46] Thus, ENMs could be used to regulate cell death through the manipulation of autophagy. One example is the enhancement of the cytotoxicity of chemotherapeutic agents by neutralizing the pro-survival effects of autophagy.[47,48] There are currently several cancer clinical trials in the US, in which the autophagy inhibitor, hydroxychloroquine, is combined with chemotherapeutic agents to enhance cancer cell killing. Nanomaterials that block autophagic flux could be considered for this role as sensitizers of chemotherapy.

Conversely, the enhancement of autophagy induction by ENMs could play a role in improving the survival of neurons that are burdened with increased removal of aggregated proteins and mitochondria in the setting of neurodegenerative disease.[17] Similarly, since many infectious pathogens (*e.g.*, the tubercle bacillus) have developed the ability to survive intracellularly by disrupting host autophagy pathways, speeding up of autophagic flux could play a role in assisting the clearance of pathogens.[47]

## CONCLUSIONS

In this work, selected ENM stimuli that lead to the activation of the NLRP3 inflammasome were used to determine whether differential effects on the autophagy pathway will influence pro-inflammatory cellular responses. Although both MWCNTs and REOs could induce NLRP3 inflammasome activation, these materials had different effects on autophagic flux. While REOs induced enhanced autophagosome accumulation, AP-MWCNTs showed no effect. The mechanism of REO-induced autophagosome accumulation involves interference in the fusion of autophagosomes with lysosomes, in part because of effects on lysosomal alkalization as well as phosphoprotein function. This study provides new insights into the potential regulatory effects of ENMs on the homeostatic regulation of the NLRP3 inflammasome.

## MATERIALS AND METHODS

**Materials.** AP-MWCNTs were purchased from Cheap Tubes. COOH-MWCNTs were synthesized by oxidizing AP-MWCNTs in mixed acids.[4] Min-U-Sil silica (quartz) was purchased from US Silica (Frederick, MD, USA). Mesoporous silica was generously provided by Dr. Jeffrey Zink, Department of Chemistry and Biochemistry at UCLA. $La_2O_3$, $Gd_2O_3$, $Sm_2O_3$, $Yb_2O_3$ nanoparticles were purchased from Nanostructured & Amorphous Materials (Houston, TX, USA). $TiO_2$ and $Bi_2O_3$ were provided by Dr. Lutz Madler at the Department of Production Engineering, University of Bremen, Germany. CQ, Sypro Ruby, Pro-Q-Diamond, LAMP-1 antibody and pHrodo were purchased from Life Technologies (Grand Island, NY, USA). 4-Methylumbelliferyl-beta-D-galactopyranoside, 3-methyladenine and Rapa were purchased from Sigma-Aldrich (St. Louis, MO, USA). Anti-LC-3 was purchased from Abcam (Cambridge, MA, USA). Anti-mTOR, anti-cathepsin D and anti-ASC antibodies were purchased from Santa Cruz Biotechnology (Dallas, Texas, USA). Recombinant human $\beta$-galactosidase was purchased from R&D (Minneapolis, MN, USA). The phosphopeptide, LPSSPVpYEDAASFK, was purchased from Apeptide (Shanghai, China). NLRP3$^{-/-}$ or ASC$^{-/-}$ THP-1 cells are prepared from THP-1 cells that transfected with NLRP3 or ASC shRNA.

**ELISA.** Aliquots of $5 \times 10^4$ wild type, NLRP3$^{-/-}$ or ASC$^{-/-}$ THP-1 cells were seeded in 96-well plates, with each well receiving 100 $\mu$L RPMI 1640 medium supplemented with 10% fetal bovine serum. 1 $\mu$g/mL phorbol 12-myristate acetate (PMA) was added to prime cells overnight before the addition of ENMs. The ENM particles were sonicated in complete RPMI 1640 medium (c-RPMI 1640), supplemented with 10 ng/mL lipopolysaccharide (LPS), at 32 W for 15 s with a sonication probe (Sonics & Materials, USA) before addition to the cells. IL-1$\beta$ release into the culture supernatants was detected by a human IL-1$\beta$ ELISA Kit (BD, CA, USA) in THP-1 cells that were exposed to the ENMs for 6–24 h at the indicated concentrations.

**Western Blotting.** Cells treated with pharmacological agents or ENMs were lysed in a buffer containing 20 mM HEPES, pH 7.4, 50 mM $\beta$-glycerophosphate, 1 mM $Na_3VO_4$, 0.5% (v/v) Triton X-100, 0.5% (v/v) CHAPS (3-[(3-cholamidopropyl)-dimethylammonio]-1-propanesulfonate hydrate) and 10% (v/v) glycerol and a cocktail of protease inhibitors. The cellular extracts were separated on a 10% or 4–10% SDS-polyacrylamide gel at 125 V and transferred to a nitrocellulose membrane at 45 V. The blotting membranes were blocked with 5% milk in PBS/Tween 20 (0.2%) for 1 h at room temperature, and then incubated with primary antibody (1/500 in blocking buffer), overnight at 4 °C. After washing four times with PBS/Tween and addition of HRP-conjugated secondary antibody (1/1000 in PBS) for 1 h at room temperature, membranes were washed four times with PBS/Tween 20 and developed with a freshly prepared luminol-based detection solution.

**Confocal Microscopy.** Control or prior treated THP-1 cells were fixed in 4% paraformaldehyde for 30 min and permeabilized by 0.2% Triton X-100 for 15 min. Permeabilized cells were subsequently incubated with primary antibodies at 4 °C overnight, followed by washing and the addition of secondary antibody or Hoechst for 2 h at room temperature. After washing, the cells were visualized under a confocal microscope (Leica Confocal SP2 1P/FCS) in the UCLA/CNSI Advanced Light Microscopy/Spectroscopy Shared Facility. High magnification images were obtained with the 63× objective.

**Use of GFP-LC3$^+$ THP-1 Cells to Study Autophagosome Assembly and Accumulation.** GFP-LC3$^+$ THP-1 cells were kindly provided by Dr. John H. Kehrl.[15] After treatment with the indicated amount of ENMs, 50–100 cells in each confocal view were counted to determine the % cells showing autophagosome accumulation. Cells were considered positive if they had more than three GFP-LC3$^+$ dots or one prominent dot. Data were presented the % GFP-LC3$^+$ cells in the population.

**2-D Gel Analysis of Lysosomal Proteins.** After incubation with each of the ENMs (50 $\mu$g/mL) for 12 h, THP-1 cells were collected for lysosome extraction using a Sigma-Aldrich kit (Lysosome Isolation). Briefly, cellular aliquots were homogenized in extraction buffer and centrifuged at 1000*g* for 10 min before collection of the supernatants. The cell pellets were discarded. After centrifugation of the extracts at 20 000*g* for 20 min, the supernatants containing cytoplasmic proteins and subcellular organelles were aspirated, while the pellets were collected and resuspended in extraction buffer. Rough endoplasmic reticulum and mitochondria were removed by adding 8 mM calcium chloride to the suspension and centrifugation at 5000*g* for 15 min. The lysosomes were isolated from the supernatants by centrifugation at 20 000*g* for 20 min, and stored at −80 °C until use.

Lysosomes were lysed in 200 $\mu$L lysis buffer and centrifuged at 15 000 rpm/min to collect the supernatants. The lysosomal proteins were precipitated by adding 1 mL 75% ethanol overnight at −20 °C. After centrifugation, the pellets were washed with cold 75% ethanol and resuspended in rehydration buffer (7 M urea, 2 M thiourea, 50 mM DTT, 4% CHAPS, 5% glycerol, 10% isopropanol, and 1% ampholytes). 100 $\mu$g lysosome protein in 200 $\mu$L rehydration buffer was applied to 11 cm, pH 3–10 IPG strips (Bio-Rad, Hercules, CA, USA). The strips were rehydrated and subjected to isoelectric focusing (IEF) as previously described (linear ramp to 100 mV over 2h, linear ramp to 250 mV in 2 h, linear ramp to 4000 mV in 5 h, hold at 4000 mV for 23 h).[48] Subsequently, the IEF strips were overlaid on an 8–16% SDS-PAGE gel. After electrophoresis, gels were stained with Pro-Q Diamond (phosphoprotein stain) and Sypro Ruby (total protein stain) and scanned in an FX Pro Plus imager (Bio-Rad). PDQuest software (Bio-Rad, version 7.2) and Same Spots ((Nonlinear Dynamics, version 3.3) software were used for 2-D image analysis.

**Use of MALDI-TOF/TOF to Determine the Phosphorylation Status of a Commercial Phosphopeptide.** The phosphopeptide (LPSSPVpYEDAASFK) was dissolved at 1 $\mu$g/$\mu$L in water. 3 $\mu$L of this solution was mixed with 75 $\mu$L of each of the ENMs ($La_2O_3$, quartz and AP-MWCNTs) dispersed at 1 mg/mL. The blank control was water only. After the incubation at 37 °C for 6 h, the peptides were analyzed by MS, carried out by a MALDI-TOF/TOF 5800 System (AB SCIEX, Foster City, CA) equipped with a 1 kHz OptiBeam on-axis laser. 2,5-Dihydroxybenzoic acid solution (25 mg/mL, in 70% ACN-$H_2O$ containing 1% $H_3PO_4$) was used as the matrix to assist the ionization of peptides.

**Assessment of $\beta$-Galactosidase Phosphorylation and Enzymatic Activity.** $\beta$-Galactosidase was diluted to 8 ng/$\mu$L in assay buffer (HCl, pH 3.5). 70 $\mu$L aliquot of this enzyme solution was added into 96-well plates, and mixed with 5 $\mu$L of 3 mg/mL ENM suspensions for 6 h incubation at 37 °C. After reaction, each of the ENM-treated suspensions was divided into two aliquots (25 and 50 $\mu$L). The 25 $\mu$L aliquot was used for mixing with 25 $\mu$L lysis buffer. After separation in 8% SDS-PAGE gel, the gel was stained by Pro-Q Diamond to examine $\beta$-galactosidase phosphorylation, followed by Sypro Ruby staining for total amount of protein. The remaining 50 $\mu$L aliquots were reacted with 50 $\mu$L of substrate solution containing 4-Methylumbelliferyl-beta-D-galactopyranoside. The fluorescence intensity of the substrate was read in kinetics mode for 30 min at excitation and emission wavelengths of 365 and 445 nm, respectively.

**Measurement of Lysosomal pH.** After treatment with 50 $\mu$g/mL of each ENM for 24 h, THP-1 cells were incubated with 50 $\mu$g/mL pHrodo green dextran in complete RPMI 1640 medium (pH, 7.4) for 4 h. Cells were washed with prewarmed, dye-free RPMI 1640 (pH 7.4) and analyzed by flow cytometry and confocal microscope. A Becton Dickinson FACS Calibur Analytic Flow cytometer in the UCLA Jonsson Comprehensive Cancer Center was used to measure pHrodo fluorescence intensity in the cells at an excitation wavelength of 488 nm.

**Obtaining BMDM and Exposure to ENMs.** After euthanasia, 6−12 week old C57BL/6 mice were sacrificed to collect the femurs by cutting tibia below the knee joints and the pelvic bone close to the hip joint. Muscles connected to the bone were removed, and the femurs were immediately placed into a tube containing sterile PBS on ice. The bones were flushed with a syringe filled with DMEM medium to extrude bone marrow, following gentle dispersion by pipet. Cell suspensions were centrifuged at 1000*g* for 5 min. The cell pellets were resuspended and differentiated in DMEM with 10% endotoxin-free fetal bovine serum (FBS) and 20% macrophage colony-stimulating factor (M-CSF) for 7 d. Then the cells were seeded in 96-well plate ($5 \times 10^4$/well) and cultured in DMEM medium plus 10% FBS, 500 ng/mL LPS for 2 d. For cytokine detection, BMDM were exposed to ENM suspensions with 10 ng/mL LPS for 24 h. After that, the supernatants were collected to determine IL-1$\beta$ using the ELISA kit described above.

**Statistical Methods.** Results were statistically analyzed using one-way ANOVA or an independent student *t* test. A statistically significant difference was regarded if the *p* value is less than 0.05. Data are reported as the mean ± standard deviation from at least three separate experiments.

*Conflict of Interest:* The authors declare no competing financial interest.

*Acknowledgment.* This work was primarily supported by the National Institute of Environmental Health Sciences, R01 ES016746. The study also leveraged the support provided by the Creative Research Group Project of NSFC (21321064), Chinese National Key Project (2012ZX10002009-011), the National Science Foundation and Environmental Protection Agency under Cooperative Agreement Number, DBI 0830117 and 1266377, and the JCCC grant, P30 CA016042. Any opinions, findings, and conclusions or recommendations expressed in this material are those of the authors and do not necessarily represent the views of the National Science Foundation, the Environmental Protection Agency or the National Institute of Health. LC3-GFP-transfected THP-1 cells were kindly provided by Ali Vural and Dr. Kehrl from the National Institute of Allergy and Infectious Diseases, National Institutes of Health.

*Supporting Information Available:* The hydrodynamic size and zeta potential of ENMs, IL-1$\beta$ production in ASC- and NLRP3-KO cells, time-response curve of autophagosome accumulation, confocal images of autophagosome accumulation in BMDM, mTOR expression, TEM images of ENMs after PSF treatment and REOs in cells, 2-D gel imaging of lysosomal phosphoproteins, and detection of lysosomal pH by flow cytometry, IL-1$\beta$ production in Rapa-treated BMDM. This material is available free of charge *via* the Internet at http://pubs.acs.org.

## REFERENCES AND NOTES

1. Sun, B.; Wang, X.; Ji, Z. X.; Li, R.; Xia, T. NLRP3 Inflammasome Activation Induced by Engineered Nanomaterials. *Small* **2013**, *9*, 1595–1607.
2. Haneklaus, M.; O'Neill, L. A. J.; Coll, R. C. Modulatory Mechanisms Controlling the NLRP3 Inflammasome in Inflammation: Recent Developments. *Curr. Opin. Immunol.* **2013**, *25*, 40–45.
3. Li, R.; Ji, Z.; Chang, C. H.; Dunphy, D. R.; Cai, X.; Meng, H.; Zhang, H.; Sun, B.; Wang, X.; Dong, J.; *et al.* Surface Interactions with Compartmentalized Cellular Phosphates Explain Rare Earth Oxide Nanoparticle Hazard and Provide Opportunities for Safer Design. *ACS Nano* **2014**, *8*, 1771–1783.
4. Li, R.; Wang, X.; Ji, Z.; Sun, B.; Zhang, H.; Chang, C. H.; Lin, S.; Meng, H.; Liao, Y. P.; Wang, M.; *et al.* Surface Charge and Cellular Processing of Covalently Functionalized Multiwall Carbon Nanotubes Determine Pulmonary Toxicity. *ACS Nano* **2013**, *7*, 2352–2368.
5. Donaldson, K.; Murphy, F. A.; Duffin, R.; Poland, C. A. Asbestos, Carbon Nanotubes and the Pleural Mesothelium: A Review of the Hypothesis Regarding the Role of Long Fibre Retention in the Parietal Pleura, Inflammation and Mesothelioma. *Part. Fibre Toxicol.* **2010**, *7*, 5.
6. Ji, Z.; Wang, X.; Zhang, H.; Lin, S.; Meng, H.; Sun, B.; George, S.; Xia, T.; Nel, A. E.; Zink, J. I. Designed Synthesis of $CeO_2$ Nanorods and Nanowires for Studying Toxicological Effects of High Aspect Ratio Nanomaterials. *ACS Nano* **2012**, *6*, 5366–5380.
7. Stern, S. T.; Adiseshaiah, P. P.; Crist, R. M. Autophagy and Lysosomal Dysfunction as Emerging Mechanisms of Nanomaterial Toxicity. *Part. Fibre Toxicol.* **2012**, *9*, 20.
8. Yu, L.; Lu, Y.; Man, N.; Yu, S. H.; Wen, L. P. Rare Earth Oxide Nanocrystals Induce Autophagy in Hela Cells. *Small* **2009**, *5*, 2784–2787.
9. Zhang, Y.; Yu, C. G.; Huang, G. Y.; Wang, C. L.; Wen, L. P. Nano Rare-Earth Oxides Induced Size-Dependent Vacuolization: An Independent Pathway from Autophagy. *Int. J. Nanomed.* **2010**, *5*, 601–609.
10. Man, N.; Yu, L.; Yu, S. H.; Wen, L. P. Rare Earth Oxide Nanocrystals as A New Class of Autophagy Inducers. *Autophagy* **2010**, *6*, 310–311.
11. Chen, Y.; Yang, L. S.; Feng, C.; Wen, L. P. Nano Neodymium Oxide Induces Massive Vacuolization and Autophagic Cell Death in Non-Small Cell Lung Cancer NCI-H460 Cells. *Biochem. Biophys. Res. Commun.* **2005**, *337*, 52–60.
12. Liu, H. L.; Zhang, Y. L.; Yang, N.; Zhang, Y. X.; Liu, X. Q.; Li, C. G.; Zhao, Y.; Wang, Y. G.; Zhang, G. G.; Yang, P.; *et al.* A Functionalized Single-Walled Carbon Nanotube-Induced Autophagic Cell Death in Human Lung Cells through Akt-TSC2-mTOR Signaling. *Cell Death Dis.* **2011**, *2*, e159.
13. Stern, S. T.; Zolnik, B. S.; McLeland, C. B.; Clogston, J.; Zheng, J.; McNeil, S. E. Induction of Autophagy in Porcine Kidney Cells by Quantum Dots: A Common Cellular Response to Nanomaterials? *Toxicol. Sci.* **2008**, *106*, 140–152.
14. Harris, J.; Hartman, M.; Roche, C.; Zeng, S. J. G.; O'Shea, A.; Sharp, F. A.; Lambe, E. M.; Creagh, E. M.; Golenbock, D. T.; Tschopp, J.; *et al.* Autophagy Controls IL-1beta Secretion by Targeting Pro-IL-1beta for Degradation. *J. Biol. Chem.* **2011**, *286*, 9587–9597.
15. Shi, C. S.; Shenderov, K.; Huang, N. N.; Kabat, J.; Abu-Asab, M.; Fitzgerald, K. A.; Sher, A.; Kehrl, J. H. Activation of Autophagy by Inflammatory Signals Limits IL-1beta Production by Targeting Ubiquitinated Inflammasomes for Destruction. *Nat. Immunol.* **2012**, *13*, 255–263.
16. Wong, E.; Cuervo, A. M. Autophagy Gone Awry in Neurodegenerative Diseases. *Nat. Neurosci.* **2010**, *13*, 805–811.

17. Levine, B.; Kroemer, G. Autophagy in the Pathogenesis of Disease. *Cell* **2008**, *132*, 27–42.
18. Zhang, H. Y.; Dunphy, D. R.; Jiang, X. M.; Meng, H.; Sun, B. B.; Tarn, D.; Xue, M.; Wang, X.; Lin, S. J.; Ji, Z. X.; *et al.* Processing Pathway Dependence of Amorphous Silica Nanoparticle Toxicity: Colloidal *vs* Pyrolytic. *J. Am. Chem. Soc.* **2012**, *134*, 15790–15804.
19. Mizushima, N. Autophagy: Process and Function. *Genes Dev.* **2007**, *21*, 2861–2873.
20. Klionsky, D. J.; Abdalla, F. C.; Abeliovich, H.; Abraham, R. T.; Acevedo-Arozena, A.; Adeli, K.; Agholme, L.; Agnello, M.; Agostinis, P.; Aguirre-Ghiso, J. A.; *et al.* Guidelines for the Use and Interpretation of Assays for Monitoring Autophagy. *Autophagy* **2012**, *8*, 445–544.
21. Bjorkoy, G.; Lamark, T.; Pankiv, S.; Overvatn, A.; Brech, A.; Johansen, T. Monitoring Autophagic Degradation of P62/Sqstm1. In *Methods in Enzymology: Autophagy in Mammalian Systems*; Klionsky, D. J., Ed.; Elsevier: Amsterdam, 2009; Vol. 452, Pt B, pp 181–197.
22. Jung, C. H.; Ro, S. H.; Cao, J.; Otto, N. M.; Kim, D. H. mTOR Regulation of Autophagy. *FEBS Lett.* **2010**, *584*, 1287–1295.
23. Shapero, K.; Fenaroli, F.; Lynch, I.; Cottell, D. C.; Salvati, A.; Dawson, K. A. Time and Space Resolved Uptake Study of Silica Nanoparticles by Human Cells. *Mol. Biosyst.* **2011**, *7*, 371–378.
24. Neves, V.; Gerondopoulos, A.; Heister, E.; Tilmaciu, C.; Flahaut, E.; Soula, B.; Silva, S. R. P.; McFadden, J.; Coley, H. M. Cellular Localization, Accumulation and Trafficking of Double-Walled Carbon Nanotubes in Human Prostate Cancer Cells. *Nano Res.* **2012**, *5*, 223–234.
25. Lu, Y.; Hao, B. X.; Graeff, R.; Wong, C. W.; Wu, W. T.; Yue, J. Two Pore Channel 2 (TPC2) Inhibits Autophagosomal-Lysosomal Fusion by Alkalinizing Lysosomal Ph. *J. Biol. Chem.* **2013**, *288*, 24247–24263.
26. Homewood, C. A.; Warhurst, D. C.; Baggaley, V. C.; Peters, W. Lysosomes, pH and Anti-Malarial Action of Chloroquine. *Nature* **1972**, *235*, 50–52.
27. Gould, G. W.; Lippincott-Schwartz, J. New Roles for Endosomes: from Vesicular Carriers to Multi-Purpose Platforms. *Nat. Rev. Mol. Cell Biol.* **2009**, *10*, 287–292.
28. Ngwa, H. A.; Kanthasamy, A.; Gu, Y.; Fang, N.; Anantharam, V.; Kanthasamy, A. G. Manganese Nanoparticle Activates Mitochondrial Dependent Apoptotic Signaling and Autophagy in Dopaminergic Neuronal Cells. *Toxicol. Appl. Pharmacol.* **2011**, *256*, 227–240.
29. Reale, M.; Vianale, G.; Lotti, L. V.; Mariani-Costantini, R.; Perconti, S.; Cristaudo, A.; Leopold, K.; Antonucci, A.; Di Giampaolo, L.; Iavicoli, I.; *et al.* Effects of Palladium Nanoparticles on the Cytokine Release from Peripheral Blood Mononuclear Cells of Palladium-Sensitized Women. *J. Occup. Environ. Med.* **2011**, *53*, 1054–1060.
30. Li, J. J.; Hartono, D.; Ong, C. N.; Bay, B. H.; Yung, L. Y. Autophagy and Oxidative Stress Associated with Gold Nanoparticles. *Biomaterials* **2010**, *31*, 5996–6003.
31. Yokoyama, T.; Tam, J.; Kuroda, S.; Scott, A. W.; Aaron, J.; Larson, T.; Shanker, M.; Correa, A. M.; Kondo, S.; Roth, J. A.; *et al.* EGFR-Targeted Hybrid Plasmonic Magnetic Nanoparticles Synergistically Induce Autophagy and Apoptosis in Non-Small Cell Lung Cancer Cells. *PLoS One* **2011**, *6*, e25507.
32. Li, H.; Li, Y.; Jiao, J.; Hu, H. M. Alpha-Alumina Nanoparticles Induce Efficient Autophagy-Dependent Cross-Presentation and Potent Antitumour Response. *Nat. Nanotechnol.* **2011**, *6*, 645–650.
33. Yu, J. X.; Li, T. H. Distinct Biological Effects of Different Nanoparticles Commonly Used in Cosmetics and Medicine Coatings. *Cell Biosci.* **2011**, *1*, 19.
34. Wei, P.; Zhang, L.; Lu, Y.; Man, N.; Wen, L. C60(Nd) Nanoparticles Enhance Chemotherapeutic Susceptibility of Cancer Cells by Modulation of Autophagy. *Nanotechnology* **2010**, *21*, 495101.
35. Lee, C. M.; Huang, S. T.; Huang, S. H.; Lin, H. W.; Tsai, H. P.; Wu, J. Y.; Lin, C. M.; Chen, C. T. C-60 Fullerene-Pentoxifylline Dyad Nanoparticles Enhance Autophagy to Avoid Cytotoxic Effects Caused by the Beta-Amyloid Peptide. *Nanomed.-Nanotechnol. Biol. Med.* **2011**, *7*, 107–114.
36. Zhang, Q.; Yang, W.; Man, N.; Zheng, F.; Shen, Y.; Sun, K.; Li, Y.; Wen, L. P. Autophagy-Mediated Chemosensitization in Cancer Cells by Fullerene C60 Nanocrystal. *Autophagy* **2009**, *5*, 1107–1117.
37. Li, C.; Liu, H.; Sun, Y.; Wang, H.; Guo, F.; Rao, S.; Deng, J.; Zhang, Y.; Miao, Y.; Guo, C.; *et al.* Pamam Nanoparticles Promote Acute Lung Injury by Inducing Autophagic Cell Death through the Akt-TSC2-mTOR Signaling Pathway. *J. Mol. Cell Biol.* **2009**, *1*, 37–45.
38. Herd, H. L.; Malugin, A.; Ghandehari, H. Silica Nanoconstruct Cellular Toleration Threshold *In Vitro*. *J. Controlled Release* **2011**, *153*, 40–48.
39. Calzolai, L.; Franchini, F.; Gilliland, D.; Rossi, F. Protein–Nanoparticle Interaction: Identification of the Ubiquitin–Gold Nanoparticle Interaction Site. *Nano Lett.* **2010**, *10*, 3101–3105.
40. Li, C. G.; Liu, H. L.; Sun, Y.; Wang, H. L.; Guo, F.; Rao, S. A.; Deng, J. J.; Zhang, Y. L.; Miao, Y. F.; Guo, C. Y.; *et al.* Pamam Nanoparticles Promote Acute Lung Injury by Inducing Autophagic Cell Death through the Akt-TSC2-mTOR Signaling Pathway. *J. Mol. Cell Biol.* **2009**, *1*, 37–45.
41. Ma, X. W.; Wu, Y. Y.; Jin, S. B.; Tian, Y.; Zhang, X. N.; Zhao, Y. L.; Yu, L.; Liang, X. J. Gold Nanoparticles Induce Autophagosome Accumulation through Size-Dependent Nanoparticle Uptake and Lysosome Impairment. *ACS Nano* **2011**, *5*, 8629–8639.
42. Wan, B.; Wang, Z. X.; Lv, Q. Y.; Dong, P. X.; Zhao, L. X.; Yang, Y.; Guo, L. H. Single-Walled Carbon Nanotubes and Graphene Oxides Induce Autophagosome Accumulation and Lysosome Impairment in Primarily Cultured Murine Peritoneal Macrophages. *Toxicol. Lett.* **2013**, *221*, 118–127.
43. Shen, S.; Kepp, O.; Kroemer, G. The End of Autophagic Cell Death? *Autophagy* **2012**, *8*, 1–3.
44. Thorburn, J.; Andrysik, Z.; Staskiewicz, L.; Gump, J.; Maycotte, P.; Oberst, A.; Green, D. R.; Espinosa, J. M.; Thorburn, A. Autophagy Controls the Kinetics and Extent of Mitochondrial Apoptosis by Regulating Puma Levels. *Cell reports* **2014**, *7*, 45–52.
45. Gump, J. M.; Staskiewicz, L.; Morgan, M. J.; Bamberg, A.; Riches, D. W. H.; Thorburn, A. Autophagy Variation within a Cell Population Determines Cell Fate through Selective Degradation of Fap-1. *Nat. Cell Biol.* **2014**, *16*, 47–54.
46. Gump, J. M.; Thorburn, A. Autophagy and Apoptosis: What Is the Connection? *Trends Cell Biol.* **2011**, *21*, 387–392.
47. Yuk, J. M.; Yoshimori, T.; Jo, E. K. Autophagy and Bacterial Infectious Diseases. *Exp. Mol. Med.* **2012**, *44*, 99–108.
48. Kang, X.; Li, N.; Wang, M.; Boontheung, P.; Sioutas, C.; Harkema, J. R.; Bramble, L. A.; Nel, A. E.; Loo, J. A. Adjuvant Effects of Ambient Particulate Matter Monitored by Proteomics of Bronchoalveolar Lavage Fluid. *Proteomics* **2010**, *10*, 520–531.
49. Kuwahara, Y.; Oikawa, T.; Ochiai, Y.; Roudkenar, M. H.; Fukumoto, M.; Shimura, T.; Ohtake, Y.; Ohkubo, Y.; Mori, S.; Uchiyama, Y.; *et al.* Enhancement of Autophagy Is A Potential Modality for Tumors Refractory to Radiotherapy. *Cell Death Dis.* **2011**, *2*, e177.
50. Li, Y. Y.; Ishihara, S.; Aziz, M. M.; Oka, A.; Kusunoki, R.; Tada, Y.; Yuki, T.; Amano, Y.; Ansary, M. U.; Kinoshita, Y. Autophagy Is Required for Toll-Like Receptor-Mediated Interleukin-8 Production in Intestinal Epithelial Cells. *Int. J. Mol. Med.* **2011**, *27*, 337–344.